Fire-Driven Trend Reversal in U.S. Ozone Exposure and Air Quality Progress

Jun Wang

jun-wang-1@uiowa.edu

University of Iowa https://orcid.org/0000-0002-7334-0490

Weizhi Deng

University of Iowa https://orcid.org/0000-0002-0258-8253

Meng Zhou

National Aeronautics and Space Administration Goddard Space Flight Center

Xi Chen

University of Iowa https://orcid.org/0000-0003-4612-4044

Xiaodong Wu

University of Iowa

Huanxin Zhang

The University of Iowa

Jason Cohen

China University of Mining and Technology

Jing Wei

University of Maryland, College Park https://orcid.org/0000-0002-8803-7056

Arlindo Da Silva

NASA/Goddard Space Flight Center, Global Modeling and Assimilation Office https://orcid.org/0000-0002-3381-4030

Guy Brasseur

Max Planck Inst. for Meteorology https://orcid.org/0000-0001-6794-9497

Claire Granier

National Oceanic and Atmospheric Administration Chemical Sciences Laboratory

Laurence Rouil

European Centre for Medium-Range Weather Forecasts

Physical Sciences - Article

Keywords:

Posted Date: August 5th, 2025

DOI: https://doi.org/10.21203/rs.3.rs-7024362/v1

Additional Declarations: There is **NO** Competing Interest.

Fire-Driven Trend Reversal in U.S. Ozone Exposure and Air Quality Progress

Weizhi Deng[1], Jun Wang[1,*], Meng Zhou[2,*], Xi Chen[1], Xiaodong Wu[3], Huanxin Zhang[1], Jason B. Cohen[4], Jing Wei[5], Arlindo da Silva[2], Guy P. Brasseur[6,7], Claire Granier[8,9], Laurence Rouil[10]

[1]Department of Chemical & Biochemical Engineering, The University of Iowa, Iowa City, IA, 52242, USA

[2]Global Modeling and Assimilation Office, NASA Goddard Space Flight Center, Greenbelt, MD, 20771, USA

[3]Department of Electrical & Computer Engineering, The University of Iowa, Iowa City, IA, 52242, USA

[4]School of Environment and Spatial Informatics, China University of Mining and Technology, Xuzhou, China

[5]Department of Atmospheric and Oceanic Science, Earth System Science Interdisciplinary Center, University of Maryland, College Park, MD, USA

[6]Atmospheric Chemistry Observations and Modeling Laboratory, National Center for Atmospheric Research, Boulder, CO, USA

[7]Environmental Modeling Group, Max Planck Institute for Meteorology, Hamburg, Germany

[8]Laboratoire d'Aérologie, CNRS, Université de Toulouse, 31013 Toulouse, France

[9]NOAA/Chemical Sciences Laboratory/CIRES, University of Colorado, Boulder, CO 80221, USA

[10]European Centre for Medium-Range Weather Forecasts, Robert-Schuman-Platz 3, 53175 Bonn, Germany

[*]Correspondence to: Jun Wang (jun-wang-1@uiowa.edu), Meng Zhou (mzhou16@umbc.edu)

Submission to

Nature

July 2025

Abstract:

Recent surge in wildfire emissions from the Western USA and Canada significantly elevates the surface ozone levels across the Continental USA, hindering regulatory compliance and undermining public health[1-5]. Here, we develop a full-coverage, long-term (2003-2023), high-resolution (1 km), daily surface ozone dataset over the Continental USA using deep learning, with strong performance in capturing exceedance events of National Ambient Air Quality Standards. Compared to benchmark Copernicus Atmosphere Monitoring Service reanalysis, the dataset captures 2.5 additional exceedance events and avoids 7.5 false alarms on average per monitoring station per year. It better resolves wildfire-driven ozone peaks spatially and temporally as compared to sparse station measurements, and enables neighborhood-scale compliance assessment, improving upon current county-scale evaluations. Our dataset reveals a reversal in national trends of ozone exposure and associated premature mortality: a decline during 2003-2013 (–0.25 ppb·year^{-1}; –2.81 deaths·million^{-1}·year^{-1}) followed by an increase during 2013-2023 (+0.10 ppb·year^{-1}; +1.22 deaths·million^{-1}·year^{-1}). The reversal is primarily driven by rising fire emissions, with the most severe fire impacts on ozone exposure and associated mortality in 2023 (2.34 ppb; 7100 premature deaths), followed by 2021 (1.64 ppb; 4900 premature deaths) and 2020 (1.49 ppb; 4300 premature deaths). While the Western USA consistently experiences high ozone levels, the fastest increase occurs in the urban Midwest. In 2023, the long-range transport of Canadian fire emissions place additional 78 million people in nonattainment zones, effectively preventing a potential 5-ppb tightening of ozone standard and erasing a decade of mitigation progress. Growing challenge in ozone regulation and public health protection is expected in the coming decades as wildfire emissions increase under a warming climate[1,6,7].

Main

Despite regulated reductions in anthropogenic emissions of ozone (O_3) precursors, observation stations indicate that policy-relevant surface O_3 levels have pleated since 2013[8], potential linked to increased fire emissions from the Western USA and Canada[2]. This stagnation poses challenges to meet and potentially tighten the 2015 USA National Ambient Air Quality Standards (NAAQS), which sets a health-based limit of 70 parts per billion (ppb) for O_3, expressed as the annual fourth highest Maximum Daily 8-hour Average (MDA8) O_3 averaged over 3 years[9]. However, efforts to inform regulatory policy are largely hindered by sparse in-situ measurements: Environmental Protection Agency (EPA) monitoring stations cover just 4% of the populated area in the Continental USA (CONUS), assuming a 10 km radius per station, and serve only 26% of the population (Figure 1a). As a result, NAAQS attainment status is often designated at the county level and even cannot be determined for many regions[10]. Furthermore, only 740 out of 1998 stations have consistent records from 2003 to 2023 (Figure 1a), limiting the representativeness of the long-term trend derived from this sparse network[11]. It also challenges the estimates of O_3 exposure and associated mortality, which require gapless MDA8 at high resolution to convolve with fine-scale population data[12,13]. Here, we employ deep learning to generate a full-coverage, high-resolution (1 km), long-term (2003-2023) daily MDA8 dataset across CONUS, with a focus on exceedance events relevant to NAAQS. We then conduct full-coverage neighborhood-scale NAAQS assessments, analyze the long-term trends of O_3 exposure and its mortality burden, and evaluate the feasibility of implementing stricter standards, providing critical insights for O_3 policy in the era of rising fire emissions.

Full-coverage O_3 mapping via deep learning

While Machine Learning (ML) has gained traction in generating gapless atmospheric datasets, long-term ML-based MDA8 datasets are not available over CONUS after 2016[14,15], missing recent years of heightened wildfire emissions[4,16]. Furthermore, existing ML studies tend to underestimate MDA8 values during extreme events (MDA8 > 70 ppb), often by 50-80%, due to training biases favoring lower values (Table S1). This underestimation is reflected in regression slopes less than unity when comparing ML predictions with observations, leading to substantial undercounting of exceedance days[17].

To address these limitations, we develop a Multi-Layer Perceptron (MLP) model with a custom cost function that emphasizes extreme events (detailed in Methodology). We benchmark its performance against the Copernicus Atmosphere Monitoring Service (CAMS) reanalysis based on out-of-sample 5-fold cross-validated results (Figures 1d-e). CAMS explains 54% of the total variability in EPA daily MDA8 measurements, with a root mean squared error (RMSE) of 11.05 ppb and a mean bias (MB) of +4.24 ppb. It tends to overestimate lower values (< 50 ppb) and underestimate extremes (>70 ppb), with a regression slope of 0.76. In contrast, MLP demonstrates significant improvements with an R^2 value of 0.88 (63.0% increase), an RMSE of 4.99 ppb (54.8% reduction), and an MB of −0.04 ppb (99.1% reduction). Importantly, MLP improves prediction of exceedance events, increasing the hit rate from 46.0% to 73.8% (+2.5 exceedance events per station per year) and reducing the false alarm ratio from 74.2% to 39.6% (−7.5 false alarms per station per year). These advancements, including a regression slope of 0.98, are crucial for evaluating NAAQS compliance, where exceedance events should not exceed 3 times per year at a given station. Out-of-station 5-fold cross-validated results further confirm the model's improvements in predicting extreme events, indicated by a regression slope of 0.90 (Figure S1).

We apply the MLP model across CONUS to produce gapless daily MDA8 estimates, enabling full-coverage NAAQS assessment (Figure 1b). The MLP results capture nonattainment urban regions in California, Arizona, Utah, Colorado, Eastern Texas, Georgia, the Lake Michigan region, and Greater New York, consistent with the EPA designation in Figure 1a. Notably, it uncovers under-monitored nonattainment regions. For instance, Western Texas and Southeastern New Mexico have been in nonattainment since 2018 due to increased oil and gas activities, as evidenced by enhanced gas flaring[18,19] and tropospheric NO_2 signals[20]. Yet, these regions remain undesignated by EPA[10], highlighting a need for expanded monitoring.

Furthermore, by incorporating fine-scale features representing local anthropogenic and biogenic emissions (See Table S2 and Methodology), the MLP captures O_3 variability at 1 km resolution, offering neighborhood-scale NAAQS assessments over traditional county-scale evaluations limited by EPA station density[10]. A zoom-in over Houston shows nonattainment areas align closely with densely populated zones (Figure 1b), informing more targeted mitigation strategies.

MLP-predicted dataset also effectively captures wildfire-driven peaks, especially in rural and remote regions underrepresented by EPA stations. Figure 1c compares the MDA8 trends during the warm season (April-September, largely corresponding to the fire season) based on sparse EPA observations with those from full-coverage MLP estimates. Full-coverage MLP results show an increasing trend of 0.25 ppb·year^{-1} since 2016, capturing the peaks in 2018, 2021 and 2023, corresponding with major wildfire years in the Western USA or Canada. In contrast, the EPA trend is nearly flat (+0.05 ppb·year^{-1}) and fails to capture the peaks in 2018 and 2021. Note that the trends from MLP results collocated with EPA sites closely match those from EPA stations, indicating that the differences in overall trends

primarily stem from differences in spatial coverage. These findings highlight the value of a long-term, full-coverage, high-resolution daily MDA8 dataset to inform O_3 policy.

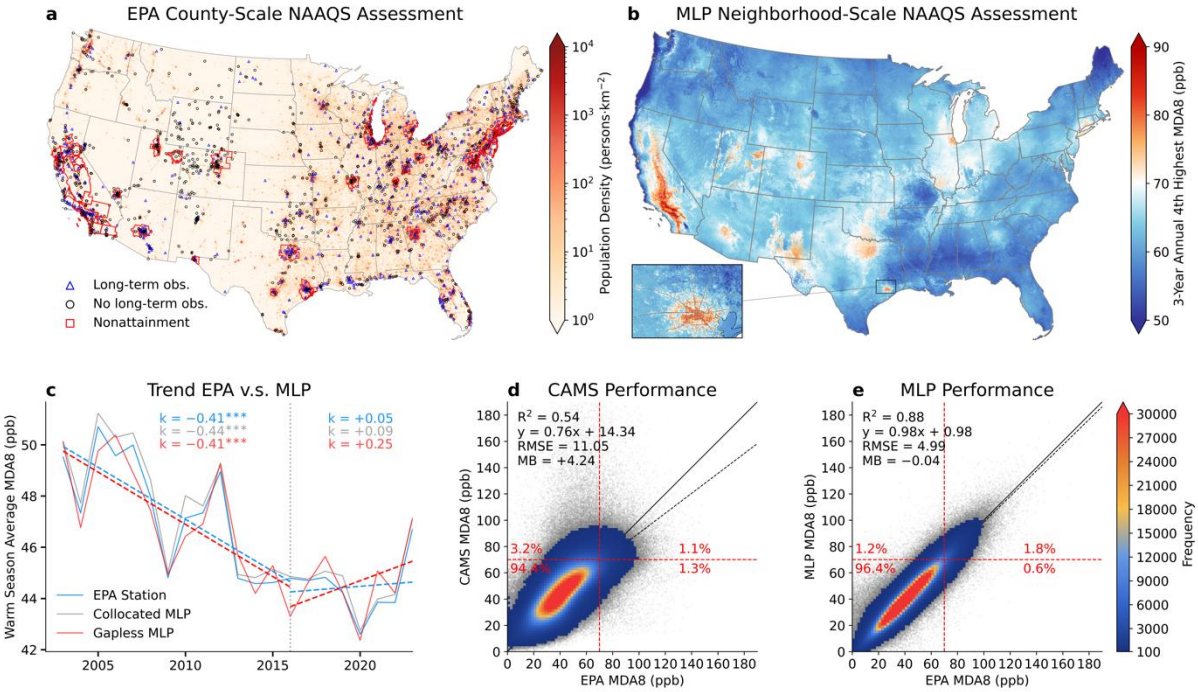

Figure 1: Need for a long-term, full-coverage, high-resolution MDA8 O_3 dataset. (a) EPA stations overlaid on LandScan population density (blue triangles: long-term observations from 2003 to 2023; black circles: no long-term observations). Red polygons show the county-scale nonattainment regions designated by EPA. **(b)** MLP-predicted annual fourth highest MDA8 averaged over 2021-2023, highlighting nonattainment regions (>70 ppb) at the neighborhood scale. **(c)** Time series and trends of warm-season MDA8 from 2003 to 2023, based on full-coverage MLP estimates (red), sparse EPA stations (blue), and MLP results collocated with EPA sites (grey). Asterisks denote significance levels of linear trends: $p < 0.1$ (*), $p < 0.05$ (**), $p < 0.01$ (***). (**d-e**) are the performance of **(d)** benchmark CAMS reanalysis and **(e)** MLP predictions, validated against EPA measurements. Black solid lines are 1:1 lines; black dashed lines are best fits; red dashed lines are the 2015 NAAQS standard; color represents data density. Results are based on out-of-sample 5-fold cross-validation.

O_3 exposure and mortality trends

We evaluate long-term O_3 exposure and associated mortality burden across CONUS from 2003 to 2023 using our MLP-predicted dataset. Previous assessments typically derive full-coverage MDA8 dataset from simple interpolation of in-situ measurements[12,21,22] or rely on outputs from Chemical Transport Models (CTMs)[13,23,24]. However, CTMs often overestimate MDA8 by 3-7 ppb, leading to inflated mortality estimates[12,25-27]. Their coarse spatial resolution further introduces uncertainties when convolved with fine-scale population data[28], whereas our high-resolution MLP dataset enables more accurate estimation of O_3 exposure and associated mortality. Our dataset also allows for long-term trend analysis for over two decades, which is particularly important as recent increase in wildfire emissions continue to exacerbate public health burden[3]. We use warm-season average MDA8 as exposure metric, consistent with the World Health Organization long-term air quality guidelines[29]. We also use it to estimate long-term O_3-attributable premature mortality (See Methodology).

While the Western USA consistently experiences high O_3 levels, we find that O_3 and associated mortality increase mostly rapidly in urban Midwest during 2013-2023. Figures 2a-f show the spatial distributions and grid-by-grid trends of the MLP-predicted warm-season average MDA8 and associated all-cause premature mortality over CONUS. O_3 levels exceeding 50 ppb (WHO long-term interim target 1) are seen in California and the Intermountain West, contributing to 200-300 annual premature deaths per million population. High O_3 levels (~50 ppb) are also found in Texas, the South Atlantic States, the Rust Belt, and the Greater New York area, with associated mortality burden of 150-200 premature deaths per million population per year. During 2003-2013, O_3 decreases at statistically significant rate (>1 ppb·year^{-1}) in California and the Southeastern USA, likely due to anthropogenic NOx reduction[30]. Most regions exhibit decreasing O_3 trends except for parts of the central USA. Correspondingly, premature mortality decreases by 2-4 deaths·million^{-1}·year^{-1} in most regions. However, grid-by-grid O_3 trends largely reverse in 2013-2023, with widespread increases exceeding 0.25 ppb·year^{-1} across the intermountain West, the Midwest, and the Gulf Coast. The increase is most pronounced in urban areas in the Midwest, where premature mortality increases sharply by 4-5 deaths·million^{-1}·year^{-1}.

National trends of O_3 exposure and associated mortality have reversed since 2013 mainly driven by increasing fire emissions. To estimate fire influence, we use CAMS surface Carbon Monoxide (CO) reanalysis as a fire proxy and exclude days with high CO levels (detailed in Methodology). The estimated fire contribution to warm-season ozone strongly correlates (Pearson R = 0.71) with the dry matter burned reported by the Global Fire Emissions Database version 4s (GFED4s) in the Western USA, demonstrating the robustness of the approach (Figure S2). The national and regional trends of O_3 exposure and associated mortality, as well as estimated fire impacts, are given in Figures 2g-l. Nationally, O_3 exposure declines by 0.25 ppb·year^{-1} during 2003-2013, leading to a premature mortality decrease of 2.81 deaths·million^{-1}·year^{-1}. In contrast, 2013-2023 sees an increasing trend of 0.10 ppb·year^{-1} in O_3 exposure and a corresponding rise in premature mortality of 1.22 deaths·million^{-1}·year^{-1}. After excluding fire impacts, these trends become nearly neutral, indicating that fire emissions are the primary driver of the reversed national trends. The largest fire-enhanced O_3 exposure and associated mortality occurs in 2023 (+2.34 ppb and +7100 premature deaths, rounded to nearest hundred), followed by 2021 (+1.64 ppb and +4900 premature deaths) and 2020 (+1.49 ppb and +4300 premature deaths).

Regional O_3 trends either reverse (e.g., Midwest) or plateau (e.g., Western USA) since 2013 due to increasing fire emissions. For regional trend analysis, we divide CONUS into the Western USA, Midwest, Northeast, and South (Figure 2a), which share similarities in their underlying geography and climate. During 2003-2013, the Midwest sees decreasing trends in O_3 exposure and associated premature mortality of 0.17 ppb·year^{-1} and 2.06 deaths·million^{-1}·year^{-1}, respectively. This reverses in 2013-2023, with increasing trends of 0.19 ppb·year^{-1} and 2.11 deaths·million^{-1}·year^{-1}, which exceed national trends. The largest fire-enhanced O_3 exposure and associated mortality occurs in 2023 (+3.32 ppb and +2100 premature deaths), followed by 2021 (+2.33 ppb and +1400 premature deaths) and 2020 (+1.67 ppb and +1000 premature deaths). After excluding high fire days, trends in the Midwest become nearly flat, suggesting the dominant role of transported wildfire emissions. In the Western USA, O_3 exposure and associated premature mortality decline by 0.19 ppb·year^{-1} and 2.31 deaths·million^{-1}·year^{-1} in 2003-2013 but then plateau during 2013-2023. After removing fire impacts, decreasing trends would resume in the second decade, indicating that the stagnation is due to elevated fire emissions. The largest fire-enhanced O_3 exposure and associated mortality occurs in 2020 (+2.41 ppb and +1600 premature deaths), followed by 2017 (+1.51 ppb and +1000 premature deaths) and 2021 (+1.38 ppb and +1000

premature deaths). These results highlight the urgent need to curb O_3 exposure and associated mortality, especially in the context of rising fire emissions that threaten to offset public health gains from anthropogenic emission reduction.

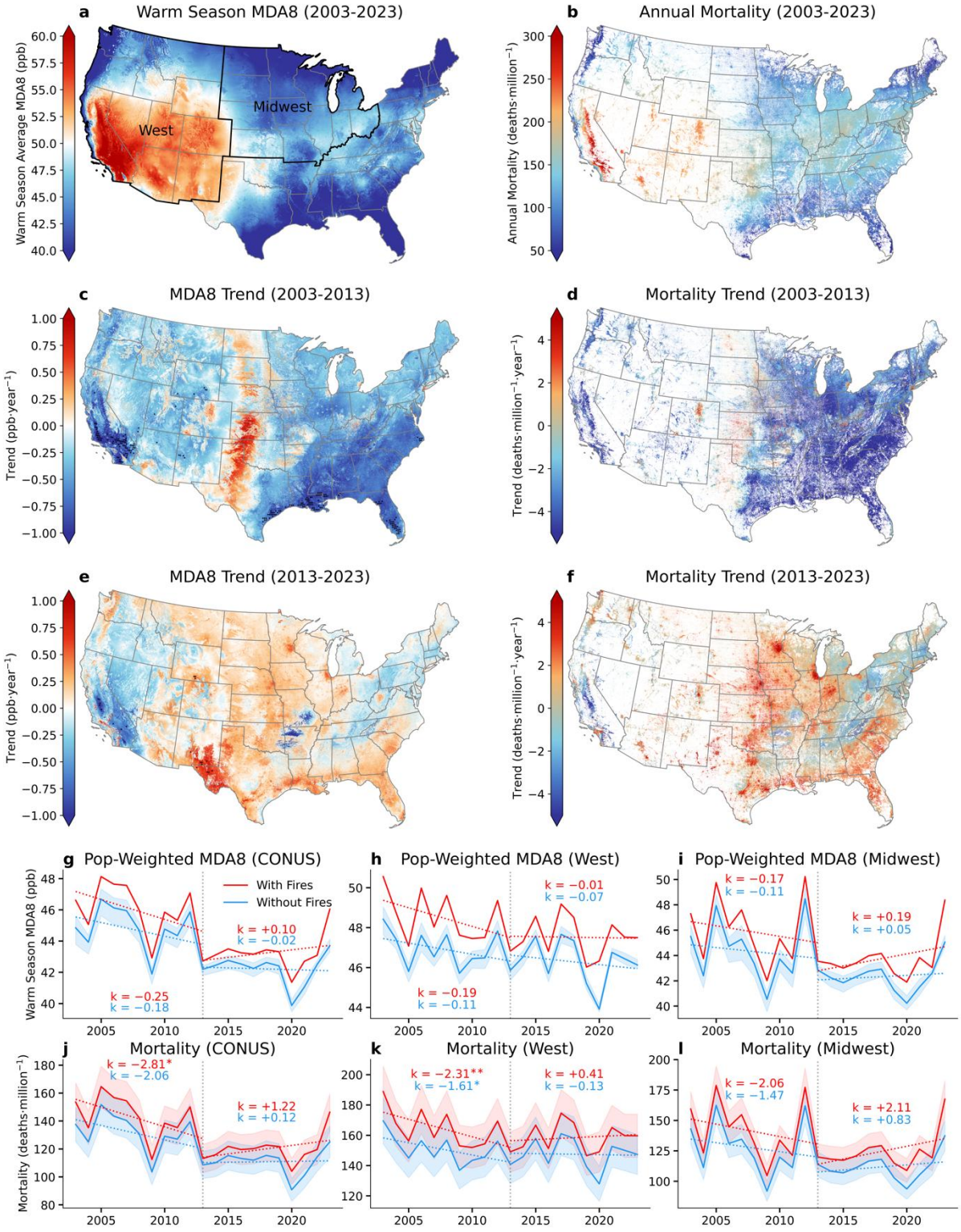

Figure 2: Spatial distributions and trends of O_3 exposure and associated premature mortality amid declining anthropogenic emissions and increasing fire emissions. (a-b) are the climatology mean during 2003-2023 of **(a)** warm-season average MDA8 and **(b)** associated annual long-term O_3-attributable all-cause premature deaths across CONUS. The

western USA and Midwest regions are highlighted in (a). **(c-d)** are the grid-by-grid trends for 2003-2013, in **(c)** warm-season MDA8 and **(d)** long-term O_3-attributable premature deaths. **(e-f)** are the same as (c-d) but for 2013-2023. Black dots indicate the trend is statistically significant at the 0.1 level. (**g-i**) are the time series and trends of population-weighted warm-season average MDA8 over (**g**) CONUS, (**h**) Western USA and (**i**) Midwest. (**j-l**) are the corresponding time series and trends of long-term O_3-attributable premature deaths (**j**) CONUS, (**k**) Western USA and (**l**) Midwest. Red lines represent MLP-predicted results; blue lines show counterfactual estimates without fire impacts; shaded areas indicate uncertainty range. Linear trend slopes are annotated, with significance levels denoted by asterisks: $p < 0.1$ (*), $p < 0.05$ (**).

Challenge in meeting and lowering O_3 standards

We assess the progress of NAAQS compliance for recent years marked by elevated wildfire emissions and examine the feasibility of lowering the current NAAQS standard. Under the current 2015 NAAQS, MDA8 should not exceed 70 ppb more than 3 days per year on average. However, epidemiological studies have reported increased mortality and morbidity even at O_3 levels below this threshold[31]. The WHO recommends a more stringent short-term O_3 guideline of 50 ppb, with an interim target of 60 ppb[29].

Figures 3a-b presents the annual exceedance days under various O_3 standards for 2020-2022 and Canadian fire-influenced year 2023. During 2020-2022, 21% of the CONUS population (70 million people) live in nonattainment areas under the currently 70 ppb standard, with 64%, 8%, and 2% exposed to at least 1 day, 1 week, and 1 month of exceedance, respectively. Southern California experiences the highest exceedance levels (>1 month), with week-long exceedances also observed in the urban areas of Arizona and Colorado, and the Permian Basin. Exceedances of more than 3 days are also common in urban Texas, the Lake Michigan region, and the New York City. If the standard was lowered to 65 ppb, 44% of the population (148 million people) would fall into nonattainment, with 87%, 23%, and 4% experiencing at least 1 day, 1 week, and 1 month of exceedance. If the standard was further lowered to 60 ppb, the proportion of population living in nonattainment zones would further increase to 75% (253 million people).

The 2023 Canadian fire smoke poses an even greater challenge to meeting and potentially lowering the O_3 standard. That year, 44% of the population (148 million people) fall into nonattainment under the 70-ppb standard, equivalent to the population in nonattainment under the 65-ppb standard in 2020-2022 (Figure 3c). Essentially, the 2023 Canadian wildfires prevent the USA from lowering O_3 standard by 5 ppb. It also offsets a decade of O_3 mitigation progress, returning compliance levels to those seen in 2011-2013 (Figure 3d). In 2023, 74%, 25%, and 2% of the population experiences at least 1 day, 1 week, and 1 month of exceedance. Widespread exceedances occur across the Midwest (>1 week), with impacts extending into the Northeast (e.g., Greater New York) and the Deep South (e.g., Texas and Georgia). Under a 65-ppb standard, 72% of the population (243 million people) would be in nonattainment, with 90%, 53%, and 8% exposed to at least 1 day, 1 week, and 1 month of exceedance. Under a 60-ppb standard, the percentage of population in nonattainment would further rise to 90% (303 million people). These results demonstrate the challenge in adopting a more stringent O_3 standard as growing wildfires contribute to high O_3 episodes.

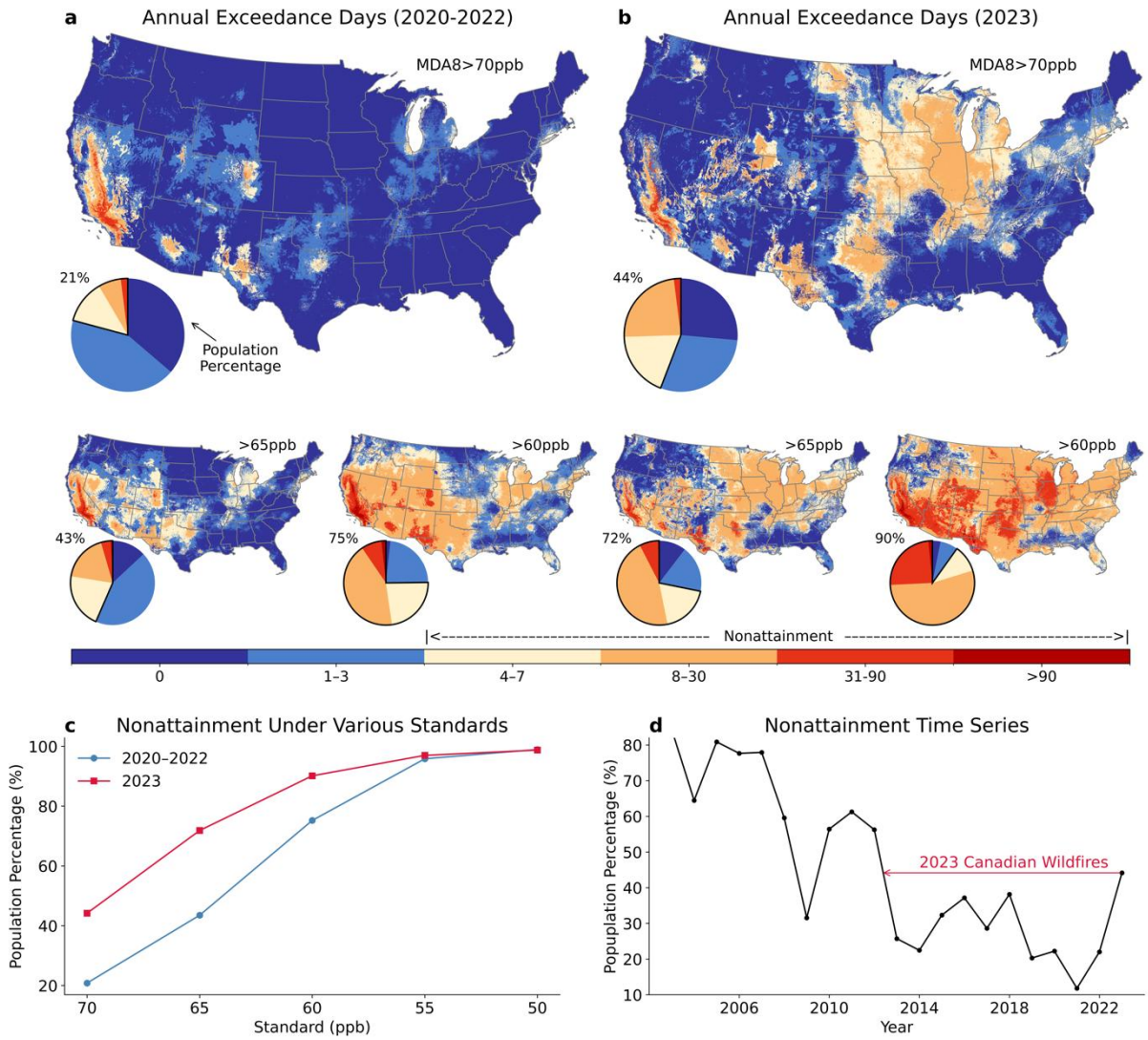

Figure 3: Challenge in meeting and lowering O_3 standards under growing fire impacts. **(a)** Average annual exceedance days during 2020-2022 under the current 2015 NAAQS (70 ppb) and hypothetical lowered standards of 65 ppb and 60 ppb. Exceedance days of 4 and above correspond to nonattainment status. Inset pie charts show the population distribution by exceedance days, with annotated percentages in nonattainment. **(b)** Same as (a) but for the Canadian fire-influenced year 2023. **(c)** Percentage of CONUS population living in nonattainment areas under different O_3 standards for 2020-2022 climatology and 2023. **(d)** Time series of percentage of CONUS population living in nonattainment areas under the current 2015 NAAQS from 2003 to 2023.

Conclusions

The recent surge in wildfire emissions from the Western USA and Canada has significantly elevated surface O_3 levels across CONUS. Yet, full-coverage MDA8 O_3 datasets remain lacking for high fire years after 2016, limiting the ability to inform regulatory policy and public health impacts. Here, we address the gap by developing a full-coverage MDA8 O_3 dataset at 1 km resolution from 2003 to 2023 using deep learning, with demonstrated strong skills in capturing exceedance events of NAAQS. Our results reveal a reversal in national trends: O_3 exposure and associated premature mortality decrease during 2003-2013 (–0.25 ppb·year^{-1} and –2.81 deaths·million^{-1}·year^{-1}) owing to declining anthropogenic emissions,

but increase during 2013-2023 (+0.10 ppb·year^{-1} and +1.22 deaths·million^{-1}·year^{-1}) largely driven by increasing fire emissions. The most significant fire enhancements in O_3 exposure and associated mortality occur in 2023 (2.34 ppb and 7100 premature deaths), followed by 2021 (1.64 ppb and 4900 premature deaths) and 2020 (1.49 ppb and 4300 premature deaths). While the Western USA consistently experiences high O_3 levels, the most rapid increases are observed in the urban Midwest. The long-range transport of Canadian fire emissions in 2023 results in additional 78 million people living in NAAQS nonattainment areas, effectively preventing the USA from tightening the O_3 standard by 5 ppb and offsetting a decade of O_3 mitigation efforts. Escalating challenge in O_3 regulation and public health protection is expected as wildfire emissions continue to rise under climate change[1,6,7]. Mitigating climate change and fire prevention measures can lead to improved standards of air quality and potentially bring large benefits to public health.

Methods

Big data for deep learning

The ML target is the EPA daily MDA8 station measurements from 2003 to 2023, aggregated to a 0.01° (~1 km) resolution. Input features are selected based on physical principles and O_3 chemistry, including datasets from model reanalysis and satellite remote sensing, all resampled to the target resolution (0.01°, daily) before training (Table S2). Key features include surface concentrations of O_3 and its precursors (i.e., nitrogen dioxide (NO_2) and formaldehyde (HCHO)) from CAMS global reanalysis[32]. Specifically, CAMS MDA8 values are derived from 3-hourly raw concentrations, which are interpolated to an hourly resolution, adjusted to local solar time, and processed using an 8-hour running average to yield 17 values a day, with the maximum representing MDA8. Given the relatively coarse resolution of CAMS global reanalysis (~75 km), high-resolution emission proxies are incorporated. For anthropogenic emissions, these proxies include LandScan population count[33] (~1 km) and Visible Infrared Imaging Radiometer Suite (VIIRS) nighttime light[34] (~375 m), the latter of which has been used to downscale NOx emissions[35]. Biogenic VOC emissions are represented using the normalized difference vegetation index (NDVI) (~1 km) from Moderate Resolution Imaging Spectroradiometer (MODIS)[36]. These fine-scale satellite products are obtained at a monthly or annual resolution, and are gap-free after temporal oversampling. Sunlight intensity, essential for driving O_3 production, is represented by all-sky shortwave down flux at the surface (~100 km), obtained from the Clouds and the Earth's Radiant Energy System (CERES)[37].

Key meteorological features, including temperature at 2 m, humidity (expressed as dew point depression at 2 m, i.e., difference between temperature and dew point), zonal and meridional wind at 10 m (~10 km resolution), and boundary layer height (~25 km), are obtained from the fifth generation European Centre for Medium-Range Weather Forecasts atmospheric reanalysis of the global climate (ERA5)[38,39]. Additional features include terrain elevation (~30 m) measured by the Advanced Spaceborne Thermal Emission and Reflection Radiometer (ASTER)[40], as high elevation regions are more susceptible to stratospheric O_3 intrusion events[41], and receive more sunlight due to less absorption from a thinner atmosphere[42], thus fostering O_3 formation. The open water fraction is determined for each 0.01° grid cell by calculating the percentage of water pixels within a 10° × 10° sliding window. High open water fraction highlights areas influenced by sea/lake breeze circulation, often associated with the high O_3 episodes due to recirculation and accumulation of O_3 and its precursors coupled with limited vertical mixing[43,44]. Auxiliary features include MODIS land use type[45] (~500 m) and day of the year. Finally, the relative feature importance is calculated using the Shapley Additive Explanations (SHAP) approach[46] (Supplementary Text S1).

MLP model with custom cost function

We employ MLP with a custom cost function to address data imbalance and improve prediction during extreme events. Data imbalance is usually tackled using techniques like over-sampling minority classes, under-sampling majority classes, or cost-sensitive learning[47,48], but awareness remains limited within the air pollution community that leverages ML[49,50]. Indeed, the histogram of EPA MDA8 measurements resembles a Gaussian distribution, although slightly right-skewed, with a mean of 41.7 ppb and a standard deviation of 13.7 ppb (Figure S3). Extreme events (MDA8 > 70 ppb) occur approximately 2 standard deviations above the mean, accounting for only 2.4% of the total measurements.

In MLP, the output target is related to input features via numerous fully-connected hidden layers[51]. Model parameters are optimized iteratively during training by minimizing the cost function, which is typically the mean squared error between ground truth (y) and MLP prediction ($\hat{y}$). However, this standard approach treats each sample equally, which may introduce bias when the dataset is imbalanced. Therefore, we design a cost function (C) based on weighted mean squared error, where rarer occurrences are given higher weights:

$$C = \frac{\sum_{k=1}^{\mathrm{N_{train}}} W_k (y_k - \hat{y}_k)^2}{\sum_{k=1}^{\mathrm{N_{train}}} W_k} \quad \text{(Eq. 1)}$$

Here, $\mathrm{N_{train}}$ is the number of training samples, y_k and $\hat{y}_k$ represent the ground truth and MLP prediction of the kth sample, and W_k is the weight of the kth sample. The weight is determined based on the Z-score, such that sample with rarer occurrences are assigned higher weights, given the distribution is "Gaussian-like":

$$W_k = e^{\frac{|Z_k|}{\gamma}} \quad \text{(Eq. 2)}$$

$$Z_k = \frac{y_k - y_{\mathrm{mean}}}{y_{\mathrm{std}}} \quad \text{(Eq. 3)}$$

In these equations, Z_k is the Z-score of the kth sample, y_{mean} and y_{std} are the mean and standard deviation of the training dataset, and γ is the weight scaling factor. In our study, γ is set to 1 after hyperparameter tuning. The weights (W_k) as a function of EPA MDA8 measurements (y_k) are shown in Figure S3. The minimum weight is 1 when EPA MDA8 measurement is 41.7 ppb (Z-score = 0). The weight increases exponentially with the absolute value of Z-score, with a value of 8.2, 24.8, and 109.2, when MDA8 is 70, 85, and 105 ppb, respectively. This custom cost function ensures that the model gives more attention to rare occurrences, including extreme highs and extreme lows, thereby improving prediction for these cases.

The MLP model is trained every year, which undergoes 5-fold cross-validation in both an out-of-sample (i.e., splitting based on all training samples) and out-of-station fashion (i.e., splitting based on EPA stations). The final models, after hyperparameter tuning, consist of a deep architecture with 9 hidden layers, each containing 1024 neurons. Stochastic gradient descent is employed for back propagation, where the batch size is set to 128 and the learning rate is initially set to 1×10^{-3} and dynamically adjusted throughout the training. The model is trained for 2500 epochs with a dropout rate of 0.1 to prevent overfitting.

Premature deaths from long-term O_3 exposure

All-cause premature deaths due to long-term O_3 exposure can be estimated as follows[12]:

$$M_{s,t} = \alpha_t \, P_{s,t} \, f_{s,t} \quad \text{(Eq. 4)}$$

where $M_{s,t}$ is the estimated number of all-cause premature deaths attributed to long-term O_3 exposure over grid s and year t, α_t is the baseline all-cause mortality rate in the US in year t, $P_{s,t}$ is the population count in grid s and year t, and $f_{s,t}$ is the attributable fraction (i.e., fraction of all-cause premature death attributable to long-term O_3 exposure) in grid s and year t. The attributable fraction is calculated as:

$$f_{s,t} = 1 - e^{-\beta \Delta X_{s,t}} \quad \text{(Eq. 5)}$$

$$\Delta X_{s,t} = \begin{cases} 0 & \text{if } X_{s,t} \le X_{\min} \\ X_{s,t} - X_{\min} & \text{if } X_{s,t} > X_{\min} \end{cases} \quad \text{(Eq. 6)}$$

where $X_{s,t}$ (ppb) is the surrogate for long-term O_3 exposure over grid s in year t, $X_{\min}$ (ppb) is the theoretical minimum risk exposure level (TMREL), and $\Delta X_{s,t}$ is the exposure level above the TMREL (ppb). β (ppb^{-1}) represents the exposure-response factor, which can be derived from the hazard ratio (HR) associated with a certain increase (ΔY) in the exposure surrogate reported by epidemiological studies:

$$\mathrm{HR} = e^{-\beta \Delta Y} \quad \text{(Eq. 7)}$$

We use warm-season average MDA8 as exposure surrogate ($X_{s,t}$) and adopt an all-cause hazard ratio of 1.011 per 10 ppb (95% CI: 1.010-1.012)[31]. A TMREL of 30.0 ppb is used as recommended by the WHO air quality guidelines[29]. Population data is obtained from LandScan[33], and baseline all-cause mortality rate in the USA is obtained from the United Nations World Population Prospects (https://population.un.org/wpp/). We apply the 2019 baseline mortality rate for the years 2020-2023 to avoid the impacts of COVID-19 on mortality trends.

Trend analysis and fire impact estimation

A decade is generally considered sufficient to attribute O_3 trends to changes in precursor emissions rather than inter-annual meteorological variations[52]. For the analysis, linear trends are determined using ordinary least squares regression, with statistical significance assessed through a two-tailed t-test. The first (2003-2013) and second (2013-2023) decade shows distinct patterns in trends, which are calculated separately.

To estimate fire contributions to O_3 levels, we conduct a sensitivity test by excluding locations and time periods influenced by fire emissions. The fire contribution is calculated as the difference between MLP-predicted O_3 levels and those obtained after removing fire influences. CO is used as a tracer for fire emissions and their downwind transport due to its role as a combustion biproduct and a long-lived O_3 precursor[53,54]. We obtain surface CO concentration from CAMS reanalysis, adjust it to local solar time, and aggregate it to a daily resolution to align with MDA8 data.

To separate fire signals from anthropogenic emissions, urban regions are first identified using an annual CO emission threshold based on the CAMS anthropogenic emission inventory[55]. Within each CONUS subregion (Figure 2a), daily CO concentration is analyzed separately for urban and non-urban amalgamations to compute the mean and standard deviation. Fire-impacted locations and time periods are identified using a cutoff set as the mean plus three standard deviations. Given the ~48% decline in USA anthropogenic CO emissions from 2003 to 2023[55], these cutoffs are adjusted annually to account for emission trends. Finally, a 10% uncertainty is applied in these cutoffs. During the fire season (April–September), locations and time periods with daily CO concentration exceeding these cutoffs are classified as fire-affected.

References:

1 Byrne, B. *et al.* Carbon emissions from the 2023 Canadian wildfires. *Nature* **633**, 835-839, doi:10.1038/s41586-024-07878-z (2024).

2 Lee, H. & Jaffe, D. A. Wildfire Impacts on O3 in the Continental United States Using PM2.5 and a Generalized Additive Model (2018–2023). *Environmental Science & Technology*, doi:10.1021/acs.est.4c05870 (2024).

3 Wei, J. *et al.* Long-term mortality burden trends attributed to black carbon and PM_{2·5} from wildfire emissions across the continental USA from 2000 to 2020: a deep learning modelling study. *The Lancet Planetary Health* **7**, e963-e975, doi:10.1016/S2542-5196(23)00235-8 (2023).

4 Cooper, O. R. *et al.* Early Season 2023 Wildfires Generated Record-Breaking Surface Ozone Anomalies Across the U.S. Upper Midwest. *Geophysical Research Letters* **51**, e2024GL111481, doi:https://doi.org/10.1029/2024GL111481 (2024).

5 Burke, M. *et al.* The contribution of wildfire to PM2.5 trends in the USA. *Nature* **622**, 761-766, doi:10.1038/s41586-023-06522-6 (2023).

6 Guardian. *LA fires forecast to be costliest blaze in US history with estimate of over $200bn in losses*, <https://www.theguardian.com/us-news/2025/jan/13/la-fires-wildfire-economic-losses> (2025).

7 NPR. *Smoke knows no boundaries: What Canada's fires mean for the U.S. in the future*, <https://www.npr.org/2025/06/06/nx-s1-5424434/wildfires-canada-u-s-climate-change> (2025).

8 USEPA. *Ozone Trends*, <https://www.epa.gov/air-trends/ozone-trends> (2024).

9 USEPA. *Review of the Ozone National Ambient Air Quality Standards*, <https://www.govinfo.gov/content/pkg/FR-2020-12-31/pdf/2020-28871.pdf> (2020).

10 USEPA. *Green Book 8-Hour Ozone (2015) Area Information*, <https://www.epa.gov/green-book/green-book-8-hour-ozone-2015-area-information> (2024).

11 Chang, K. L., McDonald, B. C., Harkins, C. & Cooper, O. R. Surface ozone trend variability across the United States and the impact of heat waves (1990–2023). *Atmos. Chem. Phys.* **25**, 5101-5132, doi:10.5194/acp-25-5101-2025 (2025).

12 Seltzer, K. M., Shindell, D. T. & Malley, C. S. Measurement-based assessment of health burdens from long-term ozone exposure in the United States, Europe, and China. *Environmental Research Letters* **13**, 104018, doi:10.1088/1748-9326/aae29d (2018).

13 Anenberg Susan, C., Horowitz Larry, W., Tong Daniel, Q. & West, J. J. An Estimate of the Global Burden of Anthropogenic Ozone and Fine Particulate Matter on Premature Human Mortality Using Atmospheric Modeling. *Environmental Health Perspectives* **118**, 1189-1195, doi:10.1289/ehp.0901220 (2010).

14 Di, Q., Rowland, S., Koutrakis, P. & Schwartz, J. A hybrid model for spatially and temporally resolved ozone exposures in the continental United States. *Journal of the Air & Waste Management Association* **67**, 39-52, doi:10.1080/10962247.2016.1200159 (2017).
15 Requia, W. J. *et al.* An Ensemble Learning Approach for Estimating High Spatiotemporal Resolution of Ground-Level Ozone in the Contiguous United States. *Environmental Science & Technology* **54**, 11037-11047, doi:10.1021/acs.est.0c01791 (2020).
16 Xu, L. *et al.* Ozone chemistry in western U.S. wildfire plumes. *Science Advances* **7**, eabl3648, doi:doi:10.1126/sciadv.abl3648 (2021).
17 USEPA. *Integrated Science Assessment for Ozone and Related Photochemical Oxidants*, <https://www.epa.gov/isa/integrated-science-assessment-isa-ozone-and-related-photochemical-oxidants> (2020).
18 Wang, J. *et al.* Detecting nighttime fire combustion phase by hybrid application of visible and infrared radiation from Suomi NPP VIIRS. *Remote Sensing of Environment* **237**, 111466, doi:https://doi.org/10.1016/j.rse.2019.111466 (2020).
19 Tran, H. *et al.* Air Quality and Health Impacts of Onshore Oil and Gas Flaring and Venting Activities Estimated Using Refined Satellite-Based Emissions. *GeoHealth* **8**, e2023GH000938, doi:https://doi.org/10.1029/2023GH000938 (2024).
20 Dix, B. *et al.* Nitrogen Oxide Emissions from U.S. Oil and Gas Production: Recent Trends and Source Attribution. *Geophysical Research Letters* **47**, e2019GL085866, doi:https://doi.org/10.1029/2019GL085866 (2020).
21 Buteau, S. *et al.* Comparison of spatiotemporal prediction models of daily exposure of individuals to ambient nitrogen dioxide and ozone in Montreal, Canada. *Environmental Research* **156**, 201-230, doi:https://doi.org/10.1016/j.envres.2017.03.017 (2017).
22 Joseph, J., Sharif, H. O., Sunil, T. & Alamgir, H. Application of validation data for assessing spatial interpolation methods for 8-h ozone or other sparsely monitored constituents. *Environmental Pollution* **178**, 411-418, doi:https://doi.org/10.1016/j.envpol.2013.03.035 (2013).
23 Malley, C. S. *et al.* Updated Global Estimates of Respiratory Mortality in Adults ≥30Years of Age Attributable to Long-Term Ozone Exposure. *Environmental Health Perspectives* **125**, 087021, doi:doi:10.1289/EHP1390 (2017).
24 Malashock, D. A. *et al.* Global trends in ozone concentration and attributable mortality for urban, peri-urban, and rural areas between 2000 and 2019: a modelling study. *The Lancet Planetary Health* **6**, e958-e967, doi:10.1016/S2542-5196(22)00260-1 (2022).
25 Zhang, Y., Olsen, K. M. & Wang, K. Fine Scale Modeling of Agricultural Air Quality over the Southeastern United States Using Two Air Quality Models. Part I. Application and Evaluation. *Aerosol and Air Quality Research* **13**, 1231-1252, doi:10.4209/aaqr.2012.12.0346 (2013).
26 Travis, K. R. *et al.* Why do models overestimate surface ozone in the Southeast United States? *Atmos. Chem. Phys.* **16**, 13561-13577, doi:10.5194/acp-16-13561-2016 (2016).
27 Appel, K. W. *et al.* Description and evaluation of the Community Multiscale Air Quality (CMAQ) modeling system version 5.1. *Geosci. Model Dev.* **10**, 1703-1732, doi:10.5194/gmd-10-1703-2017 (2017).
28 Wang, J. *et al.* Resolving and Predicting Neighborhood Vulnerability to Urban Heat and Air Pollution: Insights From a Pilot Project of Community Science. *GeoHealth* **6**, e2021GH000575, doi:https://doi.org/10.1029/2021GH000575 (2022).

29 WHO. *World Health Organization global air quality guidelines*, <https://www.who.int/publications/i/item/9789240034228> (2021).
30 Lamsal, L. N. *et al.* U.S. NO2 trends (2005–2013): EPA Air Quality System (AQS) data versus improved observations from the Ozone Monitoring Instrument (OMI). *Atmospheric Environment* **110**, 130-143, doi:https://doi.org/10.1016/j.atmosenv.2015.03.055 (2015).
31 Di, Q. *et al.* Air Pollution and Mortality in the Medicare Population. *New England Journal of Medicine* **376**, 2513-2522, doi:doi:10.1056/NEJMoa1702747 (2017).
32 Inness, A. *et al.* The CAMS reanalysis of atmospheric composition. *Atmos. Chem. Phys.* **19**, 3515-3556, doi:10.5194/acp-19-3515-2019 (2019).
33 Sims, K. *et al. LandScan Global 2022*, <landscan.ornl.gov> (2023).
34 Elvidge, C. D., Baugh, K., Zhizhin, M., Hsu, F. C. & Ghosh, T. VIIRS night-time lights. *International Journal of Remote Sensing* **38**, 5860-5879, doi:10.1080/01431161.2017.1342050 (2017).
35 Wang, Y. *et al.* Inverse modeling of SO2 and NOx emissions over China using multisensor satellite data – Part 2: Downscaling techniques for air quality analysis and forecasts. *Atmos. Chem. Phys.* **20**, 6651-6670, doi:10.5194/acp-20-6651-2020 (2020).
36 Didan, K. *MYD13A3 MODIS/Aqua Vegetation Indices Monthly L3 Global 1km SIN Grid V006*, <https://doi.org/10.5067/MODIS/MYD13A3.006> (2015).
37 Doelling, D. R. *et al.* Geostationary Enhanced Temporal Interpolation for CERES Flux Products. *Journal of Atmospheric and Oceanic Technology* **30**, 1072-1090, doi:https://doi.org/10.1175/JTECH-D-12-00136.1 (2013).
38 Muñoz Sabater, J. *ERA5-Land hourly data from 1950 to present*, <https://www.doi.org/10.24381/cds.e2161bac> (2019).
39 Hersbach, H. *et al.* The ERA5 global reanalysis. *Quarterly Journal of the Royal Meteorological Society* **146**, 1999-2049, doi:https://doi.org/10.1002/qj.3803 (2020).
40 Team, N. M. A. J. S. a. U. S. J. A. S. *ASTER Global Digital Elevation Model V003*, <https://doi.org/10.5067/ASTER/ASTGTM.003> (2019).
41 Lin, M. *et al.* Springtime high surface ozone events over the western United States: Quantifying the role of stratospheric intrusions. *Journal of Geophysical Research: Atmospheres* **117**, doi:https://doi.org/10.1029/2012JD018151 (2012).
42 Deng, W. *et al.* Advancing FRP Retrieval: Bridging Theory and Application. *IEEE Transactions on Geoscience and Remote Sensing* **62**, 1-16, doi:10.1109/TGRS.2024.3470538 (2024).
43 Cleary, P. A. *et al.* Impacts of lake breeze meteorology on ozone gradient observations along Lake Michigan shorelines in Wisconsin. *Atmospheric Environment* **269**, 118834, doi:https://doi.org/10.1016/j.atmosenv.2021.118834 (2022).
44 Geddes, J. A., Wang, B. & Li, D. Ozone and Nitrogen Dioxide Pollution in a Coastal Urban Environment: The Role of Sea Breezes, and Implications of Their Representation for Remote Sensing of Local Air Quality. *Journal of Geophysical Research: Atmospheres* **126**, e2021JD035314, doi:https://doi.org/10.1029/2021JD035314 (2021).
45 Friedl, M. & Sulla-Menashe, D. *MCD12Q1 MODIS/Terra+Aqua Land Cover Type Yearly L3 Global 500m SIN Grid V006*, <https://doi.org/10.5067/MODIS/MCD12Q1.006> (2019).
46 Scott, M. & Su-In, L. A unified approach to interpreting model predictions. *Advances in neural information processing systems* **30**, 4765-4774 (2017).
47 Chawla, N., Bowyer, K., Hall, L. O. & Kegelmeyer, W. P. SMOTE: Synthetic Minority Over-sampling Technique. *ArXiv* **abs/1106.1813** (2002).

48 Ling, C. X. & Sheng, V. S. Cost-sensitive learning and the class imbalance problem. *Encyclopedia of machine learning* **2011**, 231-235 (2008).
49 He, Q., Qin, K., Cohen, J. B., Li, D. & Kim, J. Quantifying Uncertainty in ML-Derived Atmosphere Remote Sensing: Hourly Surface NO2 Estimation With GEMS. *Geophysical Research Letters* **51**, e2024GL110468, doi:https://doi.org/10.1029/2024GL110468 (2024).
50 Petetin, H. *et al.* Model output statistics (MOS) applied to Copernicus Atmospheric Monitoring Service (CAMS) O3 forecasts: trade-offs between continuous and categorical skill scores. *Atmos. Chem. Phys.* **22**, 11603-11630, doi:10.5194/acp-22-11603-2022 (2022).
51 Chen, X. *et al.* Analytical Prediction of Scattering Properties of Spheroidal Dust Particles With Machine Learning. *Geophysical Research Letters* **49**, e2021GL097548, doi:https://doi.org/10.1029/2021GL097548 (2022).
52 Sicard, P. *et al.* Trends in urban air pollution over the last two decades: A global perspective. *Science of The Total Environment* **858**, 160064, doi:https://doi.org/10.1016/j.scitotenv.2022.160064 (2023).
53 Lin, C., Cohen, J. B., Wang, S., Lan, R. & Deng, W. A new perspective on the spatial, temporal, and vertical distribution of biomass burning: quantifying a significant increase in CO emissions. *Environmental Research Letters* **15**, 104091, doi:10.1088/1748-9326/abaa7a (2020).
54 Lin, C., Cohen, J. B., Wang, S. & Lan, R. Application of a combined standard deviation and mean based approach to MOPITT CO column data, and resulting improved representation of biomass burning and urban air pollution sources. *Remote Sensing of Environment* **241**, 111720, doi:https://doi.org/10.1016/j.rse.2020.111720 (2020).
55 Soulie, A. *et al.* Global anthropogenic emissions (CAMS-GLOB-ANT) for the Copernicus Atmosphere Monitoring Service simulations of air quality forecasts and reanalyses. *Earth Syst. Sci. Data* **16**, 2261-2279, doi:10.5194/essd-16-2261-2024 (2024).

Acknowledgements

This work was supported in part by NASA's Terra, Aqua, and SNPP Program under Award 80NNSC21L1976, by NASA's Modeling and Analysis Program (MAP) under Award 80NSSC21K1494, and by NASA's Health and Air Quality (HAQ) program under Award 80NSSC22K1047. The authors sincerely acknowledge all institutions for the public availability of their data.

Author contributions

W.D. led the machine learning development, performed data visualization and analysis, and drafted the initial manuscript. J. Wang conceptualized and supervised the research, conducted data analysis, and co-wrote the initial manuscript. M.Z. provided methodological guidance and supervision, processed ASTER and VIIRS datasets for machine learning, and contributed to data analysis. X.C., X.W., and J. Wei offered methodological guidance on machine learning. H.Z. processed MODIS datasets for machine learning. J.C., A.d., G.B., C.G., and L.R. contributed to manuscript review and revisions. All authors reviewed and approved the final manuscript.

Competing interests

The authors declare no competing interests.

Data availability

The long-term high-resolution daily surface MDA8 O_3 data generated in this study are available at https://doi.org/10.5281/zenodo.15178097. All datasets used for machine learning training are publicly available. EPA MDA8 O_3 measurements can be accessed at https://aqs.epa.gov/aqsweb/airdata/download_files.html. CAMS atmospheric composition reanalysis are downloadable at https://ads.atmosphere.copernicus.eu/datasets/cams-global-reanalysis-eac4. VIIRS nighttime light data can be downloaded at https://ladsweb.modaps.eosdis.nasa.gov/missions-and-measurements/products/VNP46A4/. LandScan population count can be downloaded at https://landscan.ornl.gov/. MODIS NDVI can be accessed at https://www.earthdata.nasa.gov/data/catalog/lpcloud-myd13a3-061. CERES shortwave flux can be downloaded at https://ceres.larc.nasa.gov/data/. ERA5 reanalysis is available at https://cds.climate.copernicus.eu/datasets/reanalysis-era5-pressure-levels?tab=download and https://cds.climate.copernicus.eu/datasets/reanalysis-era5-land?tab=download. ASTER elevation can be downloaded at https://asterweb.jpl.nasa.gov/gdem.asp. MODIS land type can be downloaded at https://ladsweb.modaps.eosdis.nasa.gov/missions-and-measurements/products/MCD12Q1.

Code availability

All data analyses and visualizations were conducted using Python. The code used in this study are available at https://github.com/uiowa-aer-lab/downscaled_cams_ozone.

Supplementary Files

This is a list of supplementary files associated with this preprint. Click to download.

- supplementozonepaper.docx